

A note on a reaction-diffusion model describing the bone morphogen protein gradient in *Drosophila* embryonic patterning

Peter van Heijster, Tasso J. Kaper and Cynthia A. Bradham

Abstract.

In this article, we consider the Eldar model [3] from embryology in which a bone morphogenic protein, a short gastrulation protein, and their compound react and diffuse. We carry out a perturbation analysis in the limit of small diffusivity of the bone morphogenic protein. This analysis establishes conditions under which some elementary results of [3] are valid.

§1. Introduction

Dorsal-ventral patterning of embryos is an important problem in the field of developmental biology. In this article, we focus on the Eldar model [3]. It is a system of three reaction-diffusion equations representing an elementary model of the evolution of the earliest stages of bone morphogenic proteins (BMPs) and other proteins in *Drosophila* embryos (fruit fly) in the dorsal region. This model helps analyze how a high BMP concentration develops around the dorsal midline, which is an essential step in the development.

The inhibitor protein short gastrulation (Sog), BMP, and the complex of these two proteins (Sog-BMP) are modeled. Let S denote the concentration of Sog, B the concentration of BMP, and C the complex

Received April 14, 2012.

Revised January 25, 2013.

2010 *Mathematics Subject Classification*. Primary 92C15, 35K57; Secondary 35Q92, 37N25, 35C20.

Key words and phrases. BMP gradients, short gastrulation, dorsal-ventral axis specification, dorsally-centered BMP concentration profiles, *Drosophila* embryo development, Eldar model, reaction-diffusion equations, singular perturbations.

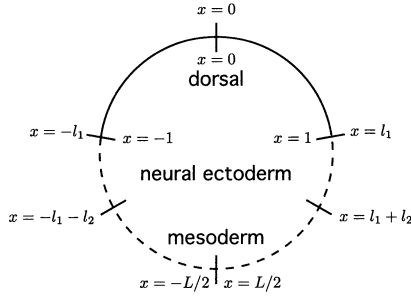


Fig. 1. Schematic depiction of the *Drosophila* embryo. The outer scale indicates the scaling of the full model. Typical values as used in [3] are $l_1 = 125\mu m$, $l_2 = 100\mu m$ and $L = 550\mu m$. The inner scale indicates the (re)scaling used in the dorsal region for this note with $x \in [-1, 1]$

Sog-BMP. The reaction-diffusion equations are given by

$$\begin{aligned}
 (1) \quad \frac{\partial S}{\partial t} &= D_S \nabla^2 S - \kappa_b SB + \kappa_{-b} C - \alpha [\text{Tld}] S, \\
 \frac{\partial B}{\partial t} &= D_B \nabla^2 B - \kappa_b SB + \kappa_{-b} C + \lambda [\text{Tld}] C, \\
 \frac{\partial C}{\partial t} &= D_C \nabla^2 C + \kappa_b SB - \kappa_{-b} C - \lambda [\text{Tld}] C.
 \end{aligned}$$

Here, D_i denotes the diffusivity of the species i , for $i = S, B, C$. Moreover κ_b is the binding rate of S to B to form the complex C and κ_{-b} is the unbinding of the complex C . The cleavage of Sog and the complex by the protein tollid [Tld] are modeled by, respectively, the cleavage parameters α and λ . Also, the concentration of [Tld] is assumed to be constant in the region of interest. The average parameter values taken for the diffusion coefficients and other parameters in [3] are

$$(2) \quad D_C = D_S = 1, D_B = 0.1, \kappa_b = 10, \kappa_{-b} = 1, \alpha [\text{Tld}] = \gamma [\text{Tld}] = 10.$$

In [3], this model is studied numerically on the interval $-l_1 \leq x \leq l_1$, where $x = 0$ represents the dorsal midline, see Fig. 1 and see also the remark in the discussion §4. Dirichlet boundary conditions are used for Sog and Sog-BMP, that is $S(\pm l_1) = s_0, C(\pm l_1) = c_0$. Moreover, symmetry is assumed around the dorsal midline: $S_x(0), C_x(0), B_x(0) = 0$. The parameters are varied over a wide range of possibilities. The

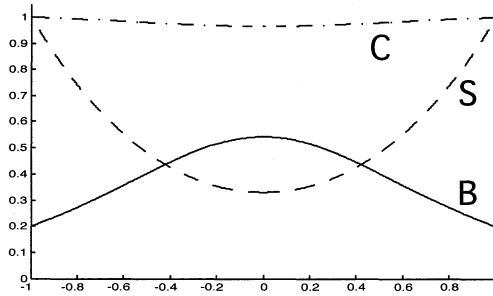


Fig. 2. A typical stationary pattern observed for (1). The system parameters are: $D_S = D_C = \kappa_{-b} = \alpha[Tld] = \lambda[Tld] = 1, D_B = 0.1$ and $\kappa_b = 10$. Note that we scaled the domain to $x \in [-1, 1]$

stationary state observed of a typical simulation is shown in Fig. 2 and note that we scaled the spatial variable to the unit domain. This is actually the scaling which we will use for x in the remainder of this article.

In [3], this model is also studied analytically under the simplifications that (i) Sog is not cleaved ($\alpha = 0$), (ii) the complex does not unbind ($\kappa_{-b} = 0$), and (iii) BMP does not diffuse, *i.e.*, $D_B = 0$. This latter simplification is motivated by the assumption that BMP has a much smaller diffusion coefficient than Sog and the compound. We remark that the magnitude of the diffusivity of BMP has been subject to much debate in the developmental biology community. See for example [1], [6], [7]. This simpler model possesses a stationary BMP concentration which is centered, and peaked, around the dorsal midline:

$$(3) \quad S(x) = \frac{\lambda[Tld]c_0}{2D_S}(x^2 + \delta^2), \quad B(x) = \frac{2D_S}{\kappa_b} \frac{1}{x^2 + \delta^2}, \quad C(x) = c_0,$$

where δ^2 depends on the system parameters and the boundary conditions. With the Dirichlet boundary conditions, we get

$$(4) \quad \delta^2 = \frac{2D_S s_0}{\lambda[Tld]c_0} - 1.$$

In this short article, we analyze a scaled version of (1) under the assumption that BMP can diffuse, but has a small diffusion coefficient. Also, all of the other parameters are allowed to have nonzero values. The main results of the analysis here include a justification of the simplifications made in [3] under an additional constraint which deals with the

smallness of the concentration of short gastrulation around the dorsal midline. We also compare our asymptotic results with results of numerical simulations of the scaled, time-independent problem obtained using the continuation package AUTO-07P [2].

§2. Asymptotic analysis of (1) in the limit of small D_B

2.1. Scalings

We first scale (1) so that we can study the influence of the small diffusion term, as well as the limits in which κ_{-b} and α go to zero. Let

$$\gamma_1 = \alpha[\text{Tld}], \quad \gamma_2 = \lambda[\text{Tld}], \quad \bar{B} = \kappa_b B, \quad \bar{x} = \frac{1}{\sqrt{D_S}} x.$$

System (1) becomes

$$(5) \quad \begin{aligned} \frac{\partial S}{\partial t} &= \nabla^2 S - S\bar{B} + \kappa_{-b}C - \gamma_1 S, \\ \frac{1}{\kappa_b} \frac{\partial \bar{B}}{\partial t} &= \frac{D_B}{\kappa_b D_S} \nabla^2 \bar{B} - S\bar{B} + \kappa_{-b}C + \gamma_2 C, \\ \frac{\partial C}{\partial t} &= \frac{D_C}{D_S} \nabla^2 C + S\bar{B} - \kappa_{-b}C - \gamma_2 C. \end{aligned}$$

Looking at the average values for κ_b, D_S, D_B and D_C taken in [3], see (2), it is reasonable to set $\frac{D_B}{D_S} = \varepsilon, \frac{D_C}{D_S} = 1$ and scale $\frac{1}{\kappa_b} = \varepsilon d$ with $d = \mathcal{O}(1)$. For convenience we take $d = 1$ and (5) becomes

$$(6) \quad \begin{aligned} \frac{\partial S}{\partial t} &= \nabla^2 S - S\bar{B} + \kappa_{-b}C - \gamma_1 S, \\ \varepsilon \frac{\partial \bar{B}}{\partial t} &= \varepsilon^2 \nabla^2 \bar{B} - S\bar{B} + \kappa_{-b}C + \gamma_2 C, \\ \frac{\partial C}{\partial t} &= \nabla^2 C + S\bar{B} - \kappa_{-b}C - \gamma_2 C. \end{aligned}$$

In order for (6) to be well-posed, we need six boundary conditions

$$(7) \quad (S(1), \bar{B}(1), C(1)) = (s_0, b_0, c_0), \quad (S_x(0), \bar{B}_x(0), C_x(0)) = (0, 0, 0).$$

2.2. Stationary solutions

In this section, we study the scaled model (6) on $(x, t) \in [0, 1] \times \mathbb{R}^+$ with $\varepsilon \ll 1$. Stationary solutions satisfy (6) with the time derivatives on the left side set to zero. There is a coefficient of ε^2 in front of the diffusion term of BMP. Hence, *a priori*, one would expect the system to be singularly perturbed with a singular limit as ε (and D_B) $\rightarrow 0$.

However, we will show that this problem is actually not singularly perturbed. Instead, for the particular solutions we examine, it is a regular perturbation problem in which the solutions limit on Eldar's solutions as $\varepsilon \rightarrow 0$, and $\kappa_{-b}, \gamma_1 \rightarrow 0$.

We introduce the regular expansions

$$(S, \bar{B}, C)(x) = (S_0, \bar{B}_0, C_0)(x) + \varepsilon^2(S_2, \bar{B}_2, C_2)(x) + \mathcal{O}(\varepsilon^3).$$

Note that since equation (6) has no explicit $\mathcal{O}(\varepsilon)$ -terms on the right hand side, we also expect that the expansions do not possess these order terms. Implementing the regular expansions we find, to leading order,

$$(8) \quad \begin{aligned} 0 &= (S_0)_{xx} - S_0 \bar{B}_0 + \kappa_{-b} C_0 - \gamma_1 S_0, \\ 0 &= -S_0 \bar{B}_0 + \kappa_{-b} C_0 + \gamma_2 C_0, \\ 0 &= (C_0)_{xx} + S_0 \bar{B}_0 - \kappa_{-b} C_0 - \gamma_2 C_0. \end{aligned}$$

This is a system of two second-order differential equations combined with an algebraic constraint. Moreover, this system is very similar to the equations analyzed in [3].

Putting the algebraic constraint of (8) into the equation for the complex C and applying the boundary conditions (7), we see that the complex is to leading order constant,

$$(9) \quad C(x) = c_0 + \mathcal{O}(\varepsilon^2).$$

Then, the equation for Sog gives

$$(S_0)_{xx} = \gamma_1 S_0 + \gamma_2 c_0.$$

The solution is

$$S_0(x) = A_1 e^{\sqrt{\gamma_1} x} + A_2 e^{-\sqrt{\gamma_1} x} - \frac{\gamma_2}{\gamma_1} c_0.$$

Using the boundary conditions (7), we obtain

$$(10) \quad S(x) = \left(s_0 + \frac{\gamma_2}{\gamma_1} c_0 \right) \operatorname{sech}(\sqrt{\gamma_1}) \cosh(\sqrt{\gamma_1} x) - \frac{\gamma_2}{\gamma_1} c_0 + \mathcal{O}(\varepsilon^2).$$

Since the Sog concentration cannot become negative, we impose

$$(11) \quad S_0(0) > 0 \quad \implies \quad (\gamma_1 s_0 + \gamma_2 c_0) \operatorname{sech}(\sqrt{\gamma_1}) - \gamma_2 c_0 > 0,$$

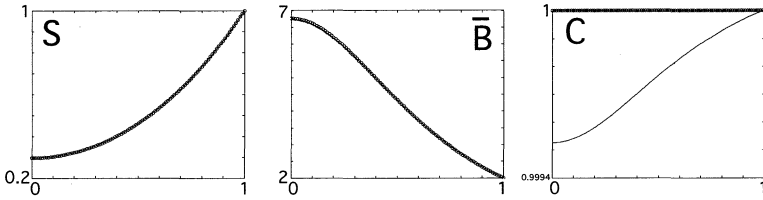


Fig. 3. Plots of the first order approximation (circles) and the solution obtained from an AUTO-07P simulation (solid line) with $s_0 = c_0 = \kappa_{-b} = \gamma_1 = \gamma_2 = 1$, $\varepsilon = 0.01$ and $b_0 = 2$ (such that (13) is fulfilled). Note the different sizes of the scales in the vertical axes, especially, for the complex C , which ranges from 0.9994 to 1.0. This difference is of $\mathcal{O}(\varepsilon^2)$

Finally, for $\bar{B}(x)$ we find

$$\begin{aligned}
 (12) \quad \bar{B}(x) &= \bar{B}_0(x) + \mathcal{O}(\varepsilon^2) = \frac{(\kappa_{-b} + \gamma_2)C_0(x)}{S_0(x)} + \mathcal{O}(\varepsilon^2) \\
 &= \frac{(\kappa_{-b} + \gamma_2)c_0}{\left(s_0 + \frac{\gamma_2}{\gamma_1}c_0\right) \operatorname{sech}(\sqrt{\gamma_1}) \cosh(\sqrt{\gamma_1}x) - \frac{\gamma_2}{\gamma_1}c_0} + \mathcal{O}(\varepsilon^2).
 \end{aligned}$$

This leading order solution agrees well with the numerically observed solutions, see Fig. 3.

At the dorsal midline $\bar{B}'(0) = 0$ as desired. However, we note that the value for BMP given by (12) at the right boundary is

$$(13) \quad \bar{B}(1) = (\kappa_{-b} + \gamma_2) \frac{c_0}{s_0} + \mathcal{O}(\varepsilon^2).$$

So, the leading order analysis is compatible with the boundary condition $\bar{B}(1) = b_0$ as long as b_0 in (7) equals $\bar{B}(1)$ in (13). Moreover, when one considers this problem on the full domain $[-L/2, L/2]$, then this compatibility condition at $\pm\ell_1$ must be satisfied by the part of the solution closer to the ventral side. On the other hand, if b_0 in (7) is different from (13), the approximation becomes inaccurate and there is a boundary layer around $x = 1$ for (6).

2.3. Peaks in $\bar{B}(x)$

High peaks in the BMP concentration around the dorsal midline arise when the denominator of $\bar{B}(x)$ is small, *i.e.*, when the Sog concentration is small at $x = 0$. This gives

$$(14) \quad (\gamma_1 s_0 + \gamma_2 c_0) \operatorname{sech}(\sqrt{\gamma_1}) - \gamma_2 c_0 \gtrsim 0.$$

In order to quantify this better, we study the “half-width” $\tilde{x} \in [0, 1]$ of the BMP component: $\bar{B}(\tilde{x}) = \frac{\bar{B}(0)}{e}$. We define

$$K_2 = \left(s_0 + \frac{\gamma_2}{\gamma_1} c_0 \right) \operatorname{sech}(\sqrt{\gamma_1}), \quad K_3 = \frac{\gamma_2}{\gamma_1} c_0, \quad K_1 = \frac{K_3}{K_2},$$

and note that (11) implies $K_2 > K_3 > 0$, which in turn implies that $0 < K_1 < 1$. Now the half-width is, to leading order,

$$\tilde{x} = \frac{\operatorname{arccosh}(e + K_1(1 - e))}{\sqrt{\gamma_1}}.$$

Since the $\operatorname{arccosh}(e + K_1(1 - e))$ is a decreasing function for $K_1 \in (0, 1)$, which approaches zero for $K_1 \rightarrow 1$, we get that the half-width \tilde{x} gets closer to zero for increasing K_1 . In other words, we can get the half-width as small as we want by choosing $K_1 \lesssim 1$, *i.e.*, by choosing $K_3 \lesssim K_2$. Note that this is similar to expression (14). So, by letting the Sog concentration go to zero at the dorsal midline, the half-width of B becomes arbitrary small.

From the above analysis, it appears that (besides the matching boundary condition (13) of BMP) a regular perturbation expansion, and thus the analysis as done in [3], gives valid approximations as long as (11) holds. Moreover, if the concentration of Sog becomes small around the dorsal midline, the leading order approximation predicts sharp peaks in BMP. However, when Sog becomes too small, the higher order terms in the regular expansion start to have an influence, see Fig. 4, and the leading approximation is thus not valid anymore. In §4, we will briefly discuss how the analysis changes when S is too small.

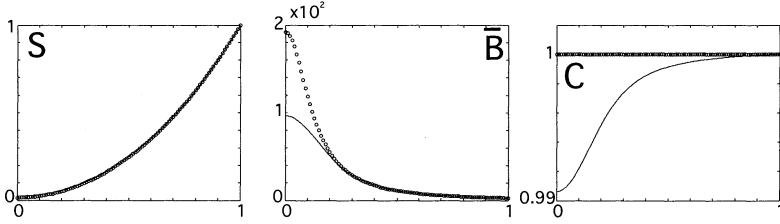


Fig. 4. Plots of the first order approximation (circles) and the solution obtained from an AUTO-07P simulation (solid line) with $s_0 = c_0 = \kappa_{-b} = \gamma_1 = 1, \gamma_2 = 1.8, \varepsilon = 0.01$ and $b_0 = 2.8$ (such that (13) is fulfilled). For these values, the left-hand side of (14) is 0.01455, which is of the asymptotic magnitude of ε . Note the different sizes of the scales in the vertical axes

2.4. Geometric analysis

We write the stationary problem of (6) as a 6-dimensional system of first order equations

$$\begin{aligned}
 s_x &= u, \\
 u_x &= sb - \kappa_{-b}c + \gamma_1 s, \\
 \varepsilon b_x &= v, \\
 \varepsilon v_x &= sb - \kappa_{-b}c - \gamma_2 c \\
 c_x &= w, \\
 w_x &= -sb + \kappa_{-b}c + \gamma_2 c.
 \end{aligned}
 \tag{15}$$

For $\varepsilon = 0$, this system has a critical 4-dimensional invariant manifold \mathcal{M}_0 given by

$$\mathcal{M}_0 = \{(s, u, b, v, c, w) : v = 0, b = \frac{(\kappa_{-b} + \gamma_2)c}{s}, s \neq 0\}.$$

The dynamics of (15) may readily be studied by examining the fast dynamics in the directions normal to \mathcal{M}_0 and the slow dynamics on the manifold \mathcal{M}_0 . We begin with the former. The fast flow, off \mathcal{M}_0 , is governed by

$$\begin{aligned}
 b_\xi &= v, \\
 v_\xi &= \bar{s}b - \kappa_{-b}\bar{c} - \gamma_2\bar{c},
 \end{aligned}
 \tag{16}$$

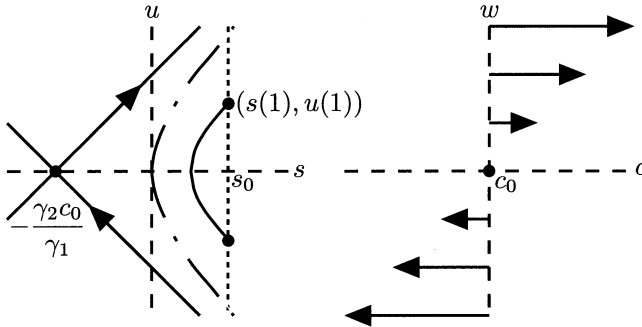


Fig. 5. The flow of (17) in the (s, u) plane and in the (c, w) plane

where \bar{s}, \bar{c} are positive constants and the variable $\xi = x/\varepsilon$ is a stretched variable. This system has a positive eigenvalue and a negative eigenvalue. Hence, in the directions normal to \mathcal{M}_0 , the fast flow is hyperbolic, with the linearization at every point on \mathcal{M}_0 having one unstable direction and one stable direction. More precisely, the manifold \mathcal{M}_0 is said to be normally hyperbolic, with one-dimensional stable fast fibers and one-dimensional unstable fast fibers.

On \mathcal{M}_0 , the dynamics is governed by

$$\begin{aligned}
 (17) \quad s_x &= u, \\
 u_x &= \gamma_1 s + \gamma_2 c, \\
 c_x &= w, \\
 w_x &= 0.
 \end{aligned}$$

This system has a double zero eigenvalue and two eigenvalues with opposite signs $\lambda^\pm = \pm\sqrt{\gamma_1}$. More specifically, the flow in the (c, w) plane is a shear flow, while the flow in the (s, u) plane is of saddle type, see Fig. 5. In this figure, condition (11) can be interpreted as follows: for given s_0 and c_0 , $u(1)$ is determined uniquely by (10), and $u(1)$ should be positive and below the dashed dotted curve, *i.e.*, the solution curve that crosses $(0, 0)$.

Since the manifold \mathcal{M}_0 is normally hyperbolic, Fenichel's persistence theorem [4], [5] implies that (15) has a locally invariant manifold \mathcal{M}_ε for ε small enough. Moreover, this manifold is $\mathcal{O}(\varepsilon)$ close to \mathcal{M}_0 . The solutions constructed in the previous sections lie on the persisting manifold \mathcal{M}_ε . Therefore, this is actually a regularly perturbed problem as long

as the concentrations of Sog and the compound are larger than $\mathcal{O}(\varepsilon^\alpha)$ with $\alpha < 1$, see Figs. 4 and 6.

Moreover, there could be solutions that approach \mathcal{M}_ε asymptotically. However, since the system of equations for BMP is linear in \bar{B} , see (16), it is not possible to construct non-trivial homoclinic solutions to \mathcal{M}_ε .

§3. Comparison with the results of [3]

To compare to the results of the elementary model in [3], we take the limit of $\gamma_1 \rightarrow 0$ in the expression of BMP (12) and also set $\kappa_{-b} = 0$. We get

$$\lim_{\gamma_1 \rightarrow 0} \bar{B}(x)|_{\kappa_{-b}=0} = \frac{2}{\frac{2s_0}{\gamma_2 c_0} + (x^2 - 1)}.$$

This is equal to Eldar's expression for BMP in (3) in the new scaling (with $D_S = 1$):

$$B(x) = \frac{2D_s}{\kappa_b} \frac{1}{x^2 + \left(\frac{2D_s s_0}{\lambda[\text{Tid}]c_0} - 1\right)} \implies \bar{B}(x) = \frac{2}{x^2 + \left(\frac{2s_0}{\gamma_2 c_0} - 1\right)}.$$

To get sharp peaks in the BMP concentration around the dorsal midline, the short gastrulation concentration must be small. This led to the condition (14). For $\gamma_1 \rightarrow 0$, condition (14) becomes

$$s_0 - \frac{\gamma_2 c_0}{2} \approx 0,$$

which is exactly the value for which the concentration of Sog vanishes at the dorsal midline. This condition is also assumed in the supplementary material of [3].

§4. Conclusion and discussion

The conclusions which can be drawn from the above analysis are twofold. First, when the concentration of Sog around the dorsal midline is not too small, the results obtained in [3] are valid. Second, these approximations are not justified anymore when this concentration does get small, see Fig. 4.

In the latter case, we need to take into account the small diffusivity of BMP and rescale (6) to the correct asymptotic magnitudes. Moreover, as shown in Fig. 6, if we choose the system parameters such that (11)

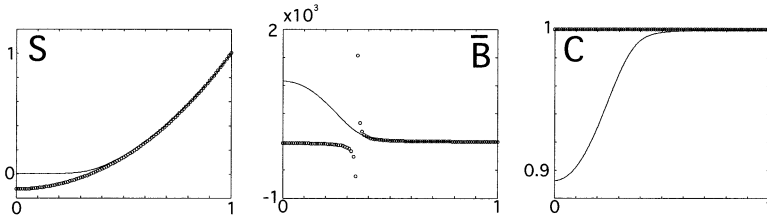


Fig. 6. Plots of the first order approximation (circles) and the solution obtained from an AUTO-07P simulation (solid line) with $s_0 = c_0 = \kappa_{-b} = \gamma_1 = 1, \gamma_2 = 2.2, \varepsilon = 0.01$ and $b_0 = 3.2$ (such that (13) is fulfilled). For these values, the left-hand side of (14) is negative, which yields the physically irrelevant case that the concentration of Sog becomes negative. The striking result is that the simulation of the full model (6) actually shows that the concentration does not become negative but is very close to zero, and that the concentration of BMP still exhibits a peak

is violated, the full model (6) still predicts peak formations for BMP around the dorsal midline. This is the subject of further research.

Finally, we remark that in [3], this elementary model (1) is also extended to a more realistic, multi-component model on the whole embryo. In later papers, see for example [6], [7], different reaction-diffusion models have been proposed to better describe and explain the embryonic patterns. These models are more complicated and harder to study analytically.

References

- [1] D. C. Clarke and X. Liu, Decoding the quantitative nature of TGF-beta/Smad signaling, *Trends in Cell Biology*, **18** (2008), 430–442.
- [2] E. J. Doedel, AUTO-07P: continuation and bifurcation software for ordinary differential equations, Tech. rep., Concordia Univ., Montreal, Canada, 2007.
- [3] A. Eldar, R. Dorfman, D. Weiss, H. Ashe, B. Z. Shilo and N. Barkai, Robustness of the BMP morphogen gradient in *Drosophila* embryonic patterning, *Nature*, **419** (2002), 304–308.

- [4] C. K. R. T. Jones, Geometric singular perturbation theory, In: Dynamical Systems, Montecatini Terme, 1994, Lecture Notes in Math., **1609**, Springer-Verlag, 1995, pp. 44–118.
- [5] T. J. Kaper, An introduction to geometric methods and dynamical systems theory for singular perturbation problems, In: Analyzing Multiscale Phenomena Using Singular Perturbation Methods, Baltimore, 1998, Proc. Sympos. Appl. Math., **56**, Amer. Math. Soc., Providence, RI, 1999, pp. 85–131.
- [6] C. M. Mizutani, Q. Nie, F. Y. M. Wan, Y. T. Zhang, P. Vilmos, R. Sousa-Neves, E. Bier, J. L. Marsh and A. D. Lander, Formation of the BMP activity gradient in the Drosophila embryo, *Developmental Cell*, **8** (2005), 915–924.
- [7] D. M. Umulis, O. Shimmi, M. B. O'Connor and H. G. Othmer, Organism-scale modeling of early Drosophila patterning via bone morphogenetic proteins, *Developmental Cell*, **18** (2010), 260–274.

Peter van Heijster
Mathematical Sciences School
Queensland University of Technology
GPO Box 2434
Brisbane, QLD 4001
Australia

Tasso J. Kaper
Department of Mathematics and Statistics
Boston University
111 Cummington Mall
Boston, MA 02215
U.S.A.

Cynthia A. Bradham
Department of Biology
Boston University
5 Cummington Mall
Boston, MA 02215
U.S.A.

E-mail address: petrus.vanheijster@qut.edu.au